buildings

MDPI

Article

Microstructure Properties of Popular Alkali-Activated Pastes Cured in Ambient Temperature

Muralidhar Kamath [1,*], Shreelaxmi Prashant [1] and Rahul Ralegaonkar [2]

[1] Department of Civil Engineering, Manipal Institute of Technology, Manipal Academy of Higher Education, Manipal, Udupi 576104, India
[2] Department of Civil Engineering, Visvesvaraya National Institute of Technology, Nagpur 440010, India; rahulrals8@gmail.com
* Correspondence: muralidhar.kamath@learner.manipal.edu

Abstract: This paper reported on the micro-level properties of alkali-activated pastes cured in ambient conditions. The mechanisms influencing setting time and the microstructure development of fly ash, slag, and metakaolin were studied. The mortar compressive strength of the binders and their ultrasonic pulse velocity (UPV) were tested after 56 days of ambient curing. The micro-level properties of paste cured at ambient conditions for seven days were determined to understand the phases developed. NASH gel was observed to delay setting and possessed lower compressive strength, while CASH gel was set early and possessed high compressive strength. The micro-characterisation of the alkali-activated binder system developed with fly ash and metakaolin showed the presence of NASH gel. The alkali-activated binder system developed with GGBS contained multiple gels, such as N, C-ASH, and CSH. The molecular structures of CSH, CASH, NASH, and N, C-ASH are also presented and were obtained using high score plus software.

Keywords: calcium oxide; aluminosilicates; Alkali activated aluminosilicates; CASH, NASH, and N, C-ASH

Citation: Kamath, M.; Prashant, S.; Ralegaonkar, R. Microstructure Properties of Popular Alkali-Activated Pastes Cured in Ambient Temperature. *Buildings* **2023**, *13*, 858. https://doi.org/10.3390/buildings13040858

Academic Editor: Bo-Tao Huang

Received: 6 March 2023
Revised: 18 March 2023
Accepted: 21 March 2023
Published: 24 March 2023

1. Introduction

Concerns about CO_2 emissions have drawn the attention of concrete researchers towards a more sustainable binder system, since OPC emits about 5–8% of total CO_2 emissions during the manufacturing process [1–3]. The alkali-activated aluminosilicate binder system is a promising material that can completely replace conventional cement (OPC) [4]. It plays a crucial role as an energy-efficient binder system because it has a lower environmental footprint than ordinary Portland cement [5–8].

Alkali-activated aluminosilicate material can be used in structural applications and other construction works. Aluminosilicate binders can reduce greenhouse emissions and energy demand by up to 73% and 43%, respectively [9]. Since the alkali-activated aluminosilicate binder is associated with lower embodied energy and environmental impacts in terms of a lower carbon contribution, and the reuse of industrial waste products and agricultural products, these binders may prove to be a novel alternative to ordinary-Portland cement [10,11].

Generally, alkali-activated aluminosilicate binders are composed of industrial wastes such as fly ash (FA), ground granulated blast furnace slag (GGBS), and metakaolin (MK). Additionally, waste from agricultural products rich in silica, such as rice husk ash, bagasse ash, and biomass ash can also be used [12,13]. Alternative waste products are used extensively due to their chemical and physical characteristics, which suit the manufacture of cement-like products. The binders are then activated using alkali metal oxides such as NaOH/KOH mixed with water glass (sodium silicate) [14–16].

However, disparities in the material design arising from the non-uniform properties of the base materials mean that the calculation of carbon emissions is quite complicated,

making the carbon footprint of the aluminosilicate binder controversial. Researchers have contradicting opinions about the efficiency of alkali-activated aluminosilicate-based materials for possible use as binders [17]. A few combinations of alkali-activated aluminosilicate binders need heat curing, making the system energy-intensive, one of the most critical challenges. The development of alkali-activated aluminosilicate products with more environmentally sustainable and affordable activators would lead to substantial cost reductions, along with a significant reduction in the detrimental impact on the environment of the cement industry, even though energy demand is a highly contested topic [18,19].

Popularly used precursors have been categorised into low calcium (FA and MK) and high-calcium aluminosilicates (GGBS). Low-calcium aluminosilicate precursors, when activated using the water glass solution, produce the chemically stable polymerised product sodium-aluminosilicate-hydrate (NASH), [20–23]. SEM and EDS techniques have shown the presence of Ca^{+2}, Na^{+2}, Si^{+4}, and Al^{+3} elements. Researchers have also calculated the Ca/Si, Ca/Al, Na/Si, and Na/Al ratios, and described the effectiveness of the binder system [24–26]. The presence of a higher proportion of Na/Si indicates the development of the NASH gel structure. SEM micro-graph has been used to understand the binder system's morphology, surface characteristics, and porosity. The silica and alumina bond appears in the wavelength range of 900–1100 cm^{-1} with FTIR [27,28].

Since they have distinct and unique features, both alkali-activated FA and GGBS gels have been used to develop non-cement binder systems. NASH gels are typically associated with delayed setting time and comparatively lower mechanical properties; however, they offer superior durability properties. With microstructure studies, the changes in the molecular structure of NASH and the development of subsequent phases can be studied [29,30]. When a low calcium system such as FA is heat cured above 50 degrees Celsius, the hardened microstructure properties are significantly improved [31–34].

High calcium aluminosilicate binders such as GGBS primarily produce calcium-aluminosilicate-hydrate (CASH) gel. Along with the CASH gel, the presence of various other types of gels, such as CSH, NASH, and (N, C)-ASH, are also developed in small amounts [35–37]. The problem associated with CASH gel is the quick setting and leaching of calcium ions from the binder system. Since CASH gel provides superior mechanical properties, it attracts many investigators across the globe. Compared to CSH gel, Ca/Al is higher in CASH gel, which typically has a lower Ca/Si ratio and a higher Si/Al ratio.

Aluminosilicate binder pastes with high-calcium aluminosilicates usually do not require heat curing. GGBS is one of the promising high-calcium aluminosilicate materials. Since multiple gels such as CSH, NASH, and (N, C)-ASH are developed on GGBS paste's alkali-activation. Each of these gels varies in properties; assessing the micro-properties and strength plays a critical role in defining its applicability. Two types of binder systems are developed in GGBS: low calcium N, C-ASH, and high calcium (N, C)-ASH, as reported by many researchers [38–40]. The amount of heat released in developing these gels also varies significantly. Heat in the binder dramatically impacts the hardened and long-term properties of the binder phases developed. Thermodynamic and hydration modelling of the aluminosilicate paste are powerful tools for studying the micro-level details of the binder system developed [41–43].

In this study, these three popular aluminosilicates, fly ash, GGBS, and Metakaolin, were selected for investigation. The low-calcium systems were FA and MK, while the high-calcium system was GGBS. Micro-level analyses were carried out for all three alkali-activated aluminosilicate pastes. The obtained results were compared to understand the differences between the phases developed in high- and low-calcium systems. Similar studies were also performed on Portland cement paste as a reference since it is a widely accepted binder system. Advanced techniques such as FE-SEM, EDS, EDS mapping, XRD, and FTIR were used to investigate the micro-level properties of low- and high-calcium aluminosilicates. XRD data analysis was carried out using high-score-plus software, while the Rietveld technique was used to identify the chemical compounds developed in each case. The high-score software also obtained the 3D molecular structure of CSH, CASH, NASH, and (C, N)-ASH.

2. Materials and Experimental Program

Setting time, hardened properties, and morphology of the alkali-activated Class F fly-ash, metakaolin, and GGBS were studied. The three aluminosilicates chosen are readily available. The physical and chemical properties of raw materials and the experimental program are discussed below.

2.1. Raw Materials

Aluminosilicate Binders

Class F fly ash was obtained from the Raichur thermal station in Karnataka, India. Metakaolin and GGBS were received from the Astraa-chemical industry, Chennai, Tamil Nadu, India. The aluminosilicate binder's particle size analysis was performed using CILAS 1064. The particle-size distribution of the studied low-calcium and high-calcium aluminosilicates is illustrated in Figure 1. The physical and chemical properties of low-calcium and high-calcium aluminosilicates are shown in Table 1. The aluminosilicate binders were found to satisfy the pozzolana activity per clauses prescribed in ASTM C618 [44].

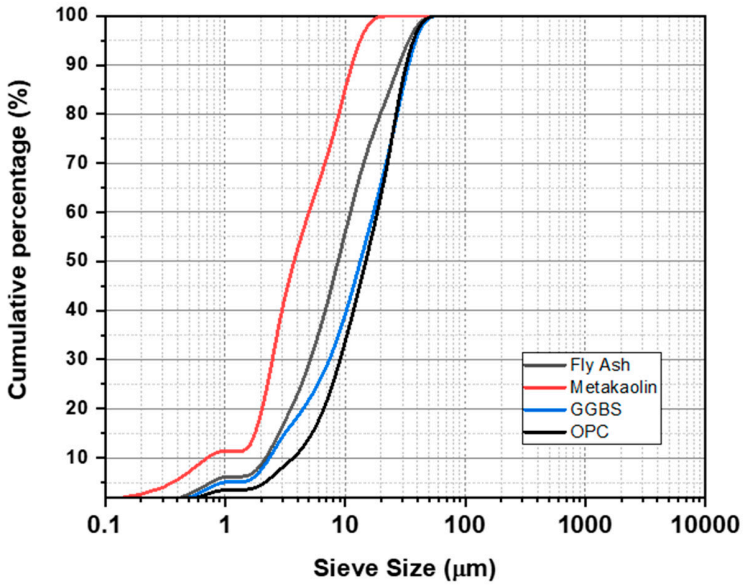

Figure 1. Particle-size distribution of binders.

Table 1. Physical and chemical properties of binders.

Materials			Fly Ash	GGBS	Metakaolin	OPC
Physical-Properties	Specific-surface area (m^2/g)		0.454	0.5	19–20	0.33
	Specific Gravity		2.24	2.67	2.6	3.15
	Particle Size(μm)	d_{10}	2.17	2.33	0.71	3.70
		d_{50}	8.72	13.37	3.75	14.83
		d_{90}	27.99	33.36	11.37	32.20
Chemical-Properties (wt.%)		SiO_2	54.11	40	52	20.21
		Al_2O_3	26.51	4.1	46	9.08
		Fe_2O_3	6.4	2	0.6	3.64
		Ca O	4.7	42	0.09	59.67
		Mg O	1.04	6.2	0.03	2.02
		SO_3	1.29	0.1	-	2.41
		Na_2O	2.22	-	0.1	-
		K_2O	0.87	-	0.03	-
		TiO_2	-	-	0.65	0.45
		LOI	2.85	0.25	-	1.45

Phases of the aluminosilicate binders were plotted as a 3D ternary diagram, as shown in Figure 2, a handy tool to compare CaO, SiO_2, and Al_2O_3 in the aluminosilicates selected for the present study. Table 2 shows that the OPC's highest calcium oxide is present while

the lowest is in the MK. About 42% of calcium oxide is present in GGBS against 4.7% in fly ash. The FESEM (field emission scanning electron microscopy) of the binders (Figure 3) indicated that the morphology of the aluminosilicate materials differ from each other in that fly-ash is spherical, while GGBS exhibits angular morphology and metakaolin appears flaky. Cement exhibits a combination of angular and flaky morphology. XRD (X-ray diffraction) of the aluminosilicate materials is shown in Figure 4.

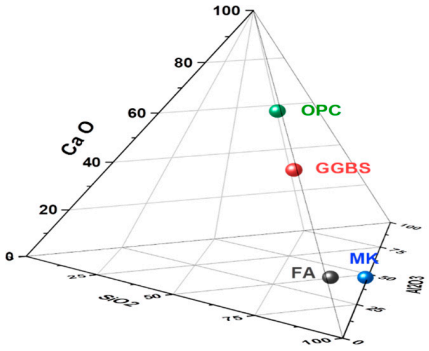

Figure 2. 3D Ternary Diagram of Aluminosilicate binders.

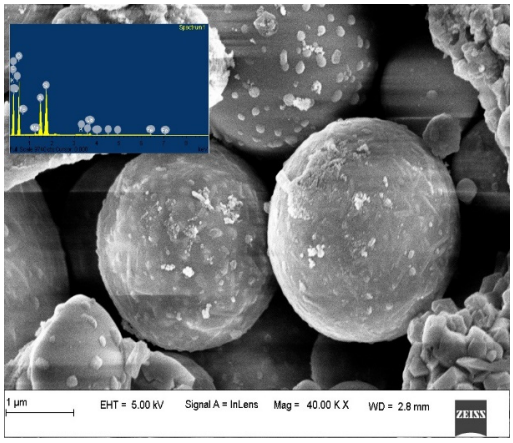

(**a**) fly-ash

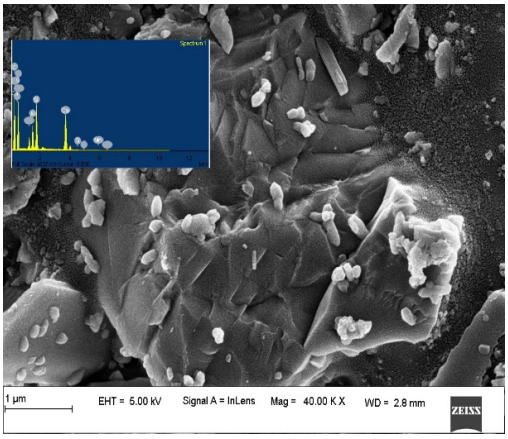

(**b**) GGBS

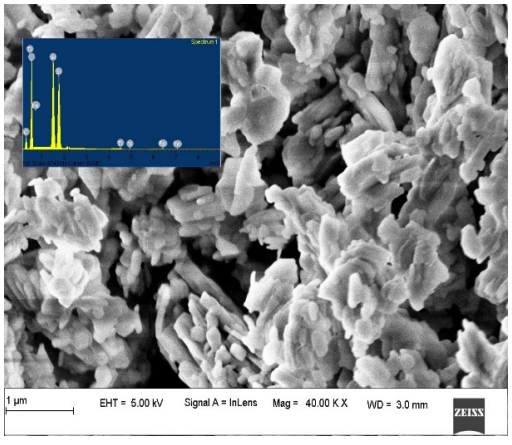

(**c**) metakaolin

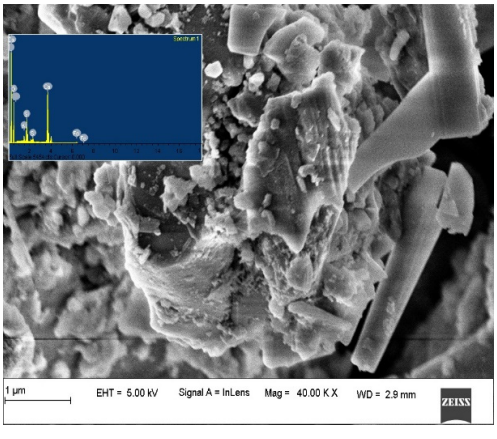

(**d**) ordinary Portland cement

Figure 3. FE-SEM images of aluminosilicate materials.

EDS spectroscopy of the aluminosilicate materials studied is shown in Figure 3. EDS mapping of aluminosilicate material is illustrated in Figure 5. EDS mapping identified calcium, silica, and alumina in the FA, MK, GGBS, cement, and other minor elements. From Figure 5, the strongest calcium intensity is noticed in the cement, followed by GGBS and FA, while there is no calcium found in metakaolin. The EDX elements of the aluminosilicate

binders are tabulated in Table 2. Si/Al ratios of OPC, GGBS, FA and MK are 4.25, 2.03, 1.57 and 0.97, respectively, whereas the Ca/Si ratios are 3.54, 1.14, 0.06 and 0.00, respectively. The ca/Al ratio is 15.02 in cement, the highest amongst the samples studied, while in GGBS, it was found to be 2.31, and in FA and MK, it was 0.

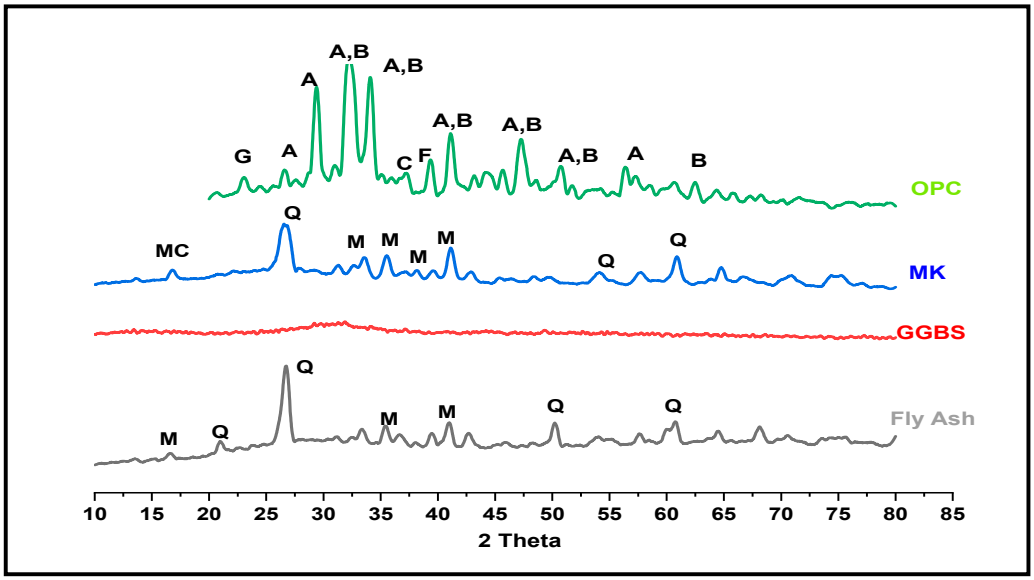

Figure 4. XRD of aluminosilicate materials.

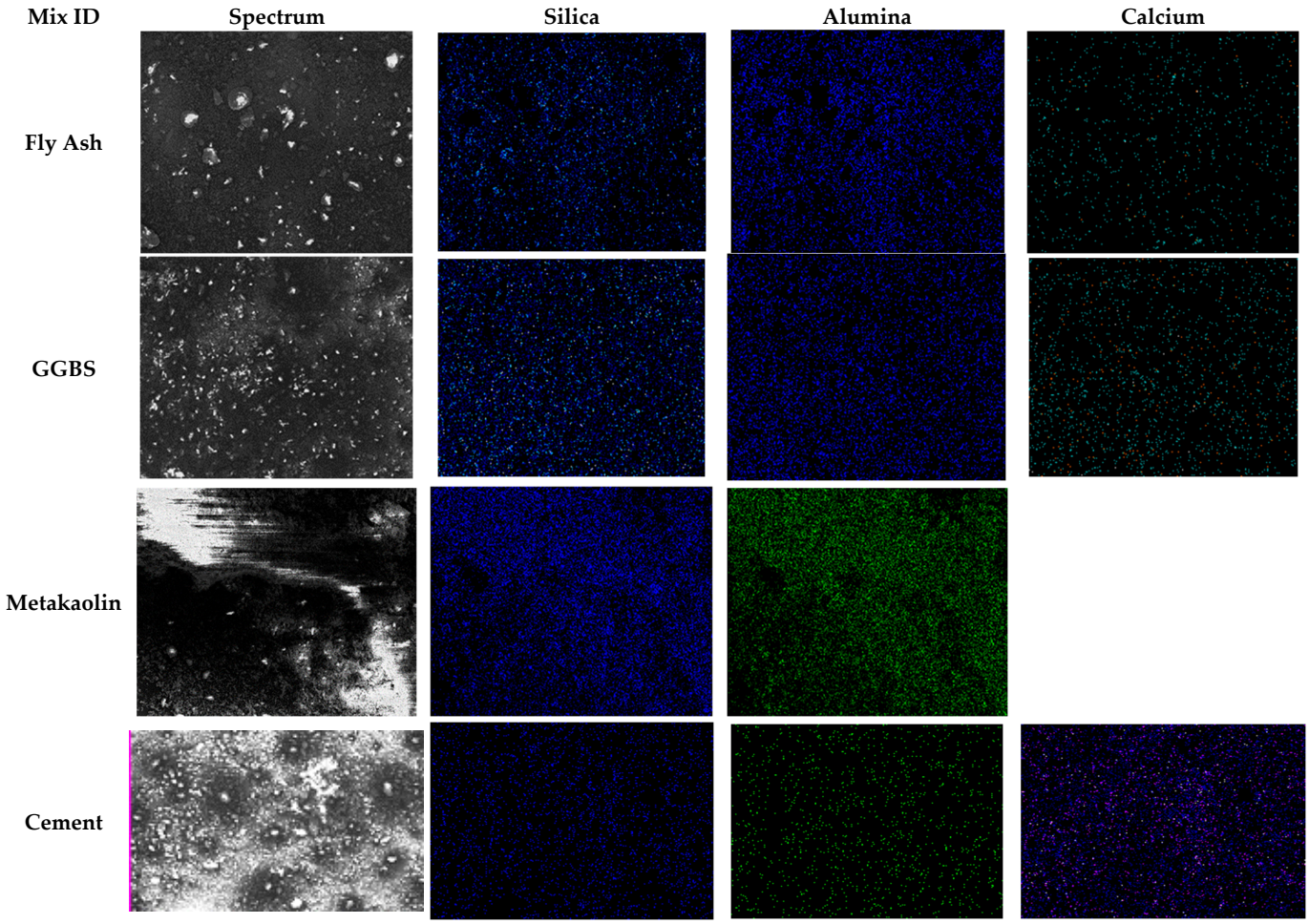

Figure 5. EDS mapping of elements of aluminosilicate materials.

Table 2. EDX elements composition of aluminosilicate binder.

Binders	Chemical Element (% by wt.) and, Their Ratio											
	Mg	**Al**	**Si**	**Ca**	**Ti**	**Fe**	**S**	**Mn**	**K**	**Si/Al**	**Ca/Si**	**Ca/Al**
OPC	-	0.84	3.57	12.62	-	0.86	0.51	-	-	4.25	3.54	15.02
GGBS	1.88	3.41	6.91	7.91	0.14	-	-	0.18	-	2.03	1.14	2.31
FA	0.28	6.07	9.53	0.6	0.25	0.78	-	-	0.28	1.57	0.06	0.098
MK	-	9.63	9.35	-	0.23	0.22	-	-	-	0.97	0.00	0

2.2. Water Glass Solution

The water glass solution of 12 molarity and sodium hydroxide to water glass ratio is 2.5. The detail of the solution used in this study refers to our previously published article [43]. In Table 3, the proportion of SS/SH and S/B ratio are tabulated.

Table 3. Alkali-activated pastes studied.

Mix ID	Designation	Content (%)	Alkali(M)	SH/SS	S/B	T (°C)
1	FA	100	12	2.5	0.35	Ambient
2	GGBS	100	12	2.5	0.35	Ambient
3	MK	100	12	2.5	0.35	Ambient
4	OPC	100	-	-	0.35	Moist

2.3. Aluminosilicate Paste

Pastes of aluminosilicates such as FA, GGBS, and MK were prepared, along with OPC in the proportions mentioned in Table 3. The alkaline liquid-to-binder ratio of 0.35 was applied for all paste sample preparations. The specimens, cast in three-dimensional moulds of 40 cubic millimetres, were used for characterisation at the micro-level. The samples were removed from moulds after 1 day, and ambient cured until testing. Cement paste was cured underwater at ambient conditions.

2.4. Alkali-Activated-Aluminosilicate Mortar

Alkali-activated mortar of 3 aluminosilicate mixes and cement paste were prepared in the proportions mentioned in Table 3. Alkali-activated mortar contained 1 part of binder and 3 parts of fine aggregate by weight. Standard fine-aggregate with a specific gravity of 2.65 was used to cast the mortars, according to IS 383-2016 [45]. The alkali-activated mortar cube specimens were cast in cubic moulds of 70.6 mm.

2.5. Experimental Program

2.5.1. Fresh Properties of Paste

One of the essential characteristics of binder materials is Vicat time. The initial and final times of the alkali-activated-paste were calculated using the Vicat by the ASTM-C191 [46] specification.

2.5.2. Mechanical Properties of Mortar

Mortar cubes were tested for compressive strength as per clause of ASTM-C109 [47] on the 3rd, 7th, 28th, and 56th day of curing. A UPV test was also conducted on the 3rd, 7th, 28th, and 56th days of curing, as per ASTM-C597 [48].

2.5.3. Micro-Level Properties of Paste

The microstructure studies using FESEM, EDS, EDS mapping, XRD, and FTIR were performed at 7 days for the aluminosilicate pastes. Table 4 provides a summary of the experimental programme.

Table 4. Experimental Program.

Sl. No.	Parameter Studied	Standards/Instrument
1	Setting time	ASTM C191 [46]
2	Compressive strength	ASTM C109 [47]
3	UPV	ASTM C597 [48]
4	FESEM	Carl Zeiss FESEM, Oxford Instrument
5	EDS	Carl Zeiss FESEM, Oxford Instrument
6	XRD	Rigaku Mini flex
7	FTIR	JASCO FT/IR-6300

3. Results and Discussion

3.1. Setting Properties of Alkali-Activated FA, GGBS, and MK Pastes

The setting time test was performed using the Vicat apparatus for three popular binders fly ash, GGBS, MK, and OPC pastes. The initial setting time of fly-ash, GGBS, MK, and OPC pastes are 450, 70, 110, and 95 min, respectively. The final setting time of the fly-ash, GGBS, MK, and OPC pastes were 810, 115, 150, and 295 min, respectively. The initial and final setting times were noted at 5 min intervals, as illustrated in Figure 6. The calcium oxide content in the alkali-activated fly-ash, metakaolin, and GGBS pastes were 4.7, 0.09, 42%, respectively, and the OPC paste is 59.67%. The setting time was found to be significantly influenced by the calcium content. Alkali-activated fly ash, metakaolin, and GGBS contain higher calcium content exhibited faster-setting characteristics.

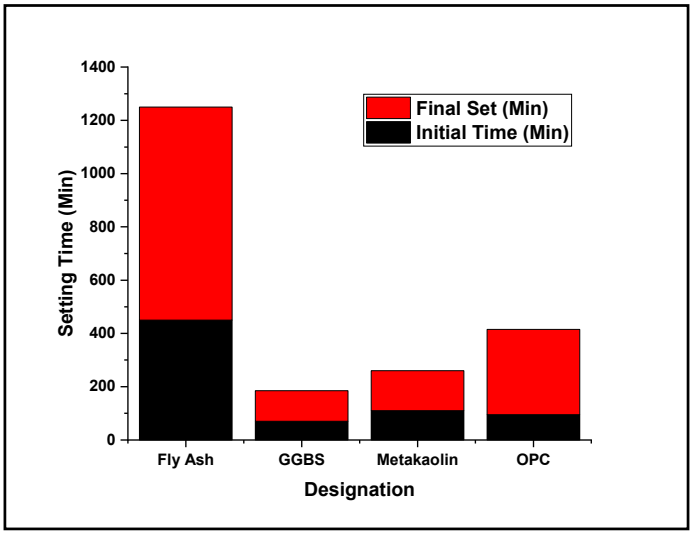

Figure 6. Initial & Final-setting time of pastes.

Studies by Dai et al. (2020) have reported the initial setting time of alkali-activated fly ash as 13, and more than 18 h for the pastes with a solution-to-binder ratio of 0.27 and 0.37, respectively. With the introduction of slag into the system, the calcium increases in the system, and the setting time reduces significantly [49]. The gel present in alkali-activated GGBS paste is mainly calcium/sodium aluminate silicate hydrate (CaO/Na_2O-Al_2O_3-SiO_2-H_2O), and in the OPC paste it is primarily the calcium silicate hydrates (CaO-SiO_2-H_2O). CASH exhibits faster-setting characteristics in comparison with CSH due to bounded water between the molecules. The final setting times noticed for GGBS and OPC pastes were 115 and 295 min, respectively.

Almakhadmeh et al. (2021) investigated how water temperature affected the setting of alkali-activated slag paste. The setting time was observed to be decreased by the water's temperature [50]. Additionally, OPC final-setting-time is higher due to gypsum (calcium sulphate dihydrate) in OPC. In alkali-activated fly ash and metakaolin, the gels developed are primarily the sodium aluminate silicate hydrate (Na_2O-Al_2O_3-SiO_2-H_2O). NASH gel

requires more time to set, which is observed in the case of fly-ash paste. NASH gel is developed because of polymerization and possesses a 3D tetrahedral structure and cross-linked chain. If NASH gel is supplemented with heat, the setting may be enhanced [51–53]. A chemical element such as calcium oxide may be introduced in the binder system to liberate heat and strengthen the setting characteristics. On the other hand, the binder's surface area and fineness also play a vital role that can be noticed in the metakaolin paste. In the sections on FESEM, XRD, and FTIR, the critical characteristics of the gel are addressed in considerable detail.

3.2. Mechanical Properties

3.2.1. Alkali-Activated-Mortar-Compressive-Strength

Alkali-activated fly ash, GGBS, and MK mortar were tested for compressive strength after curing for 3, 7, 28, and 56 days in the ambient conditions and compared with the strength of OPC mortar water cured at ambient conditions. Figure 7 shows a plot of the mortars' tested compressive strength. The compressive strength of alkali-activated fly-ash, GGBS, and MK mortar at 56 days is 48.22, 54.65, and 32.42 MPa, respectively, and of the OPC mortar is 58.14 MPa. The compressive strengths of alkali-activated fly ash, GGBS, and MK mortar are 17.06%, 6%, and 44.32%, respectively, lower than the strength of the OPC mortar.

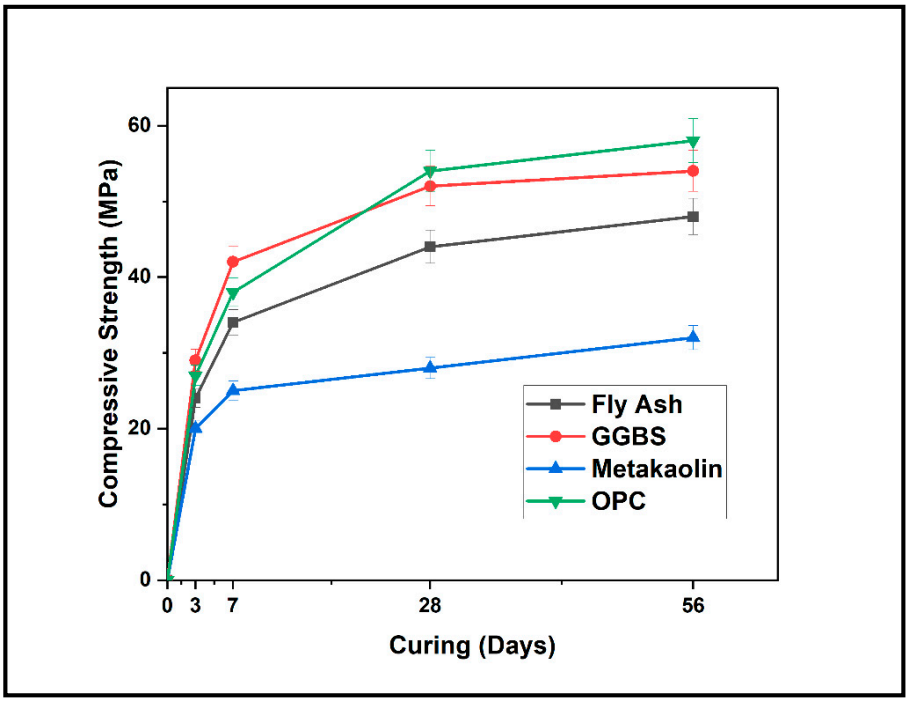

Figure 7. Compressive strength of mortar at 3rd, 7th, 28th and 56th days.

The alkali-activated fly-ash and MK binders developed lower compressive-strength than the alkali-activated GGBS compared to the OPC's reference [54–56]. The mortar compressive strength at seven days of FA, GGBS, and MK were 34.18, 42.24, and 25.64 MPa, respectively, while the OPC mortar was 38.35 MPa. The FA and MK mortar compressive strengths were 12.20% and 49.57%, respectively, lower than that of the OPC mortar, while the GGBS mortar strength increased to 10.14%. NASH, as the primary reaction product of alkali-activated FA and MK types of gel, has lower compressive strength than alkali-activated GGBS. CASH gel exhibited early compressive strength, and later strength is lower than other gels such as CSH and NASH. However, NASH is chemically more stable when related to CASH, while in CASH, leaching of calcium was observed. Hence, NASH is more durable than calcium-based gel [57]. Cercel et al. (2020) studied the alkali-activated slag

mortar with the inclusion of quartz (glass powder) with the binary activator of hydrated lime and sodium-carbonate. Alkali-activated-slag mortar exhibits better mechanical and microstructure properties [58].

3.2.2. Alkali-Activated Mortar UPV Results

The UPV results for the aluminosilicates tested on the mortar samples are shown in Figure 8. The UPV values for alkali-activated fly ash, GGBS, and MK mortar were 3166, 4020, and 2676 m/s after 56th days of air curing, while after the seventh day of curing, UPV values were 2456, 3352, and 2346 m/s. The UPV value of OPC mortar at 56 and seven days were 3689 and 3057 m/s.

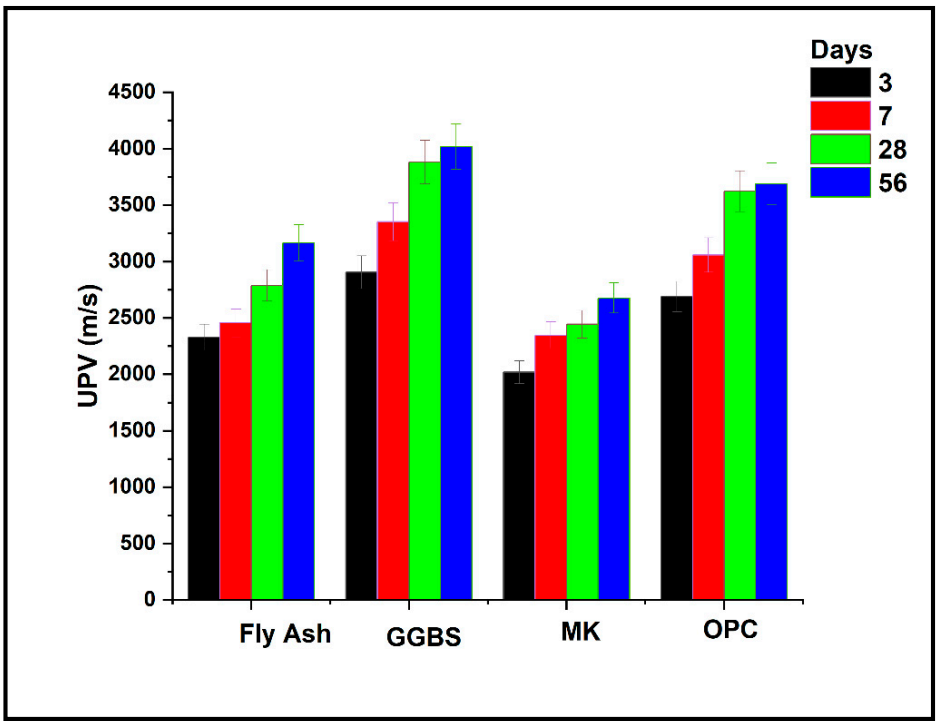

Figure 8. UPV of Mortar at 3, 7, 28 and 56 days.

UPV values of all the alkali-activated FA, GGBS and MK binder mortar samples improved with curing duration till 28 days. A high-calcium alkali-activated GGBS mortar showed the highest UPV values due to multiple gels and the interaction of compounds to produce a dense microstructure. Higher UPV values of the alkali-activated GGBS binder system indicate a higher density than low-calcium binder systems such as alkali-activated FA and MK. Lower UPV values in low-calcium binders indicate poor interlinking between the compounds produced. The lowest UPV value was noted in the MK-based alkali-activated mortar. The compressive strength of the mortar specimen likewise showed a similar type of observed trend. Farhan et al. 2019 elaborated on the mechanical properties of alkali-activated fly ash and GGBS mortar. The UPV values of mortar range from 300 to 2400 m/s at 7th & 28th days of curing. The reported UPV results align with previously published works [7,59–62].

3.3. Microstructure of Alkali-Activated FA, GGBS, and MK

3.3.1. Alkali-Activated FA, GGBS, and MK Studied Using FE-SEM

FE-SEM analysis was performed to understand the morphology, structure, nature, density, and orientation of cracks and the pore system of low-calcium and high-calcium binder systems. Figures 9 and 10 display FE-Sem micrographs with scales of 20 micro-meter and 1.0 KX resolution and 1 m and 10.0 KX resolution, respectively.

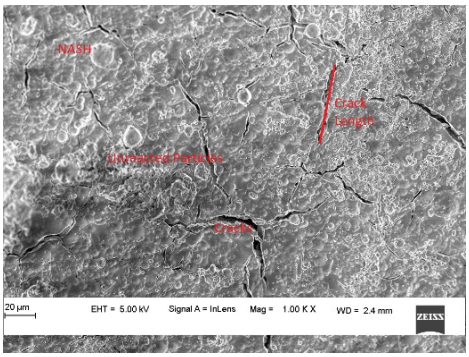

(**a**) fly-ash paste

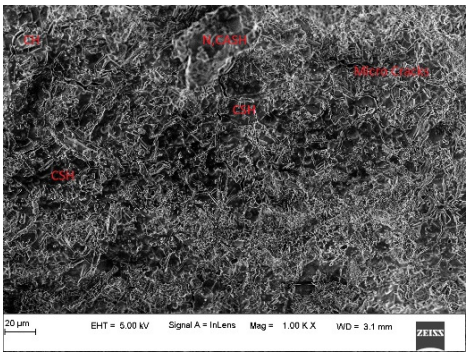

(**b**) GGBS paste

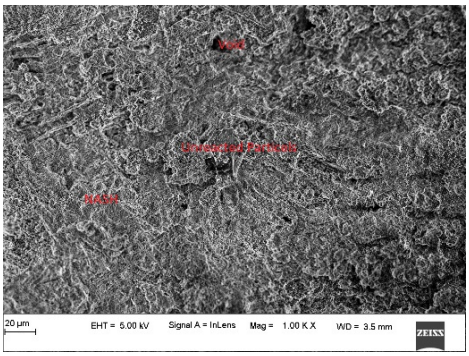

(**c**) metakaolin paste

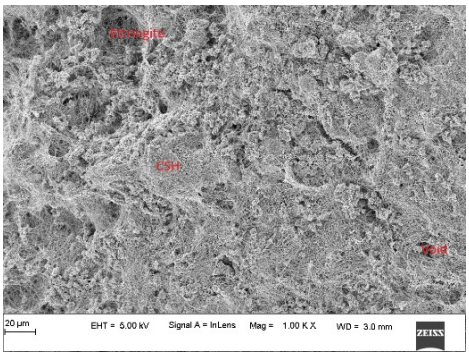

(**d**) OPC paste

Figure 9. Alkali-activated paste at 7 days with magnification 1KX.

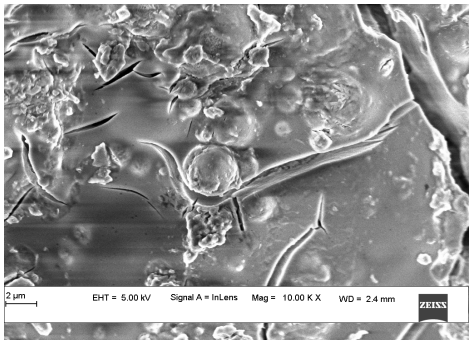

(**a**) Fly-Ash Paste

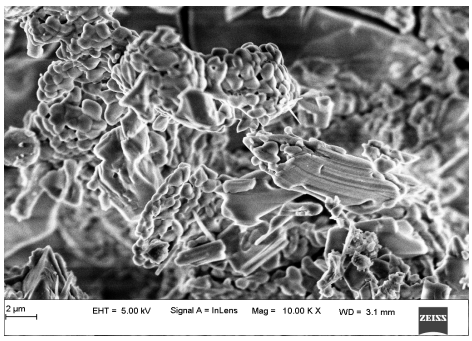

(**b**) GGBS Paste

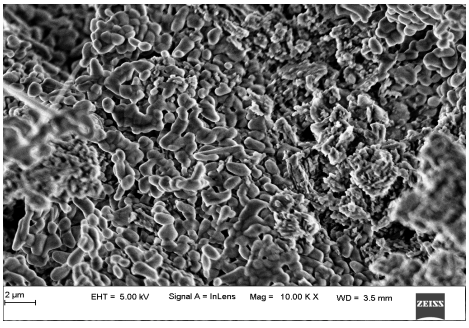

(**c**) metakaolin paste

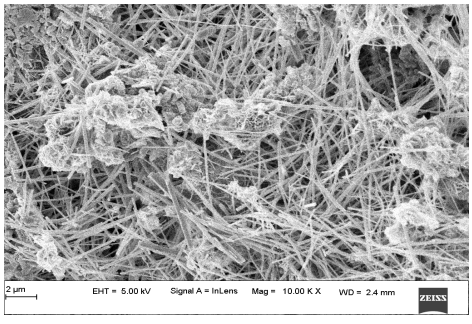

(**d**) OPC paste

Figure 10. Alkali-activated paste at 7th days with magnification 10 KX.

Activation of the starting raw binders resulted in phases that displayed completely different morphologies, as observed in the FE-SEM images (Figures 9 and 10). The alkali-activated fly ash and metakaolin paste contain low $ca^{2+,}$ while high ca^{2+} appeared in the alkali-activated GGBS and OPC pastes. The alkali-activated GGBS is denser compared to

the alkali-activated FA and MK. The 3D dimensional cross-linked structure of NASH gel is developed in the alkali-activated FA and MK pastes. CSH, CASH, and NASH gels are formed in the activated GGBS paste. In the OPC paste, CSH gel is produced due to the hydration of calcium and silica.

OPC paste can be compact and dense, with fewer cracks and tiny pores. The presence of calcium hydroxide (Ca $(OH)_2$) flakes is observed in GGBS paste while there is almost negligible FA and MK. MK paste is observed to be least dense with fragmented compounds and unreacted particles. OPC paste is denser among all the pastes studied, while the alkali-activated GGBS paste is denser than the FA and MK paste. The alkali-activated fly ash has a higher crack length than other pastes studied. Furthermore, the NASH gel (a three-dimensional structure) is more stable than calcium-based gel types [63–65].

3.3.2. Alkali-Activated FA, GGBS, and MK Studied Using EDS

Energy dispersive spectroscopy (EDS) and mapping were explored to understand the chemical composition of low-calcium alkali-activated (fly ash and MK) and high-calcium alkali-activated (alkali-activated GGBS and OPC) pastes. The EDS elements are tabulated in Table 5. The elemental spectrum of pastes is shown in Figure 11. Elements identified in alkali-activated FA, and MK pastes were Na, Si, Al, and Ca. The GGBS paste contained insignificant Na, Si, Al, and Ca proportions. For the OPC paste, the elements present were Si, Al, and a high ratio of Ca was observed in the binder system.

Table 5. EDS analysis of alkali-activated paste.

Mixes	Spectrum	Elements (% by wt.) and Their Ratio											
		Na	Al	Si	Ca	Si + Al	Si/Al	Ca/ (Si + Al)	Na/ (Si + Al)	Ca/Si	Na/Al	Na/Si	Ca/Al
FA	1	5.84	3.08	9.57	0.36	12.65	3.11	0.03	0.46	0.04	1.90	0.61	0.12
	2	6.04	3.2	9.97	0.37	13.17	3.12	0.03	0.46	0.04	1.89	0.61	0.12
GGBS	1	8.88	1.77	5.42	1.63	7.19	3.06	0.23	1.24	0.30	5.02	1.64	0.92
	2	9.06	1.97	5.47	1.58	7.44	2.78	0.21	1.22	0.29	4.60	1.66	0.80
MK	1	2.97	6.37	7.46	0.02	13.83	1.17	0.00	0.21	0.00	0.47	0.40	0.00
	2	4.84	6.18	7.21	0.02	13.39	1.17	0.00	0.36	0.00	0.78	0.67	0.00
OPC	1	0.12	1.07	4.34	15.14	5.41	4.06	2.80	0.02	3.49	0.11	0.03	14.15
	2	0	1.09	4.41	15.31	5.50	4.05	2.78	0.00	3.47	0.00	0.00	14.05

Lothenbach et al., 2019 have, through studies, reported that the Ca/Si ratio of the C, N-ASH is closer to 1 and an Al/Si ratio lower than less than 0.25 [66]. Table 5 shows the EDS analysis of the pastes studied. The alkali-activated FA paste, with one area spectrum, shows the Ca/(Si + Al) and Na/(Si + Al) ratios as 0.04 and 0.46, respectively. The ratios Ca/Si, Na/Al, Na/Si, and Ca/Al are 0.04, 1.90, 0.61, and 0.12, respectively. The ratio of elements indicated the presence of the NASH gel binder system, and the area 2 spectrum is almost similar. The alkali-activated GGBS paste with one area spectrum showed the Ca/(Si + Al) ratio and Na/ (Si + Al) as 0.23 and 1.24, respectively, while the Ca/Si, Na/Al, Na/Si and Ca/Al ratios were 0.30, 5.02, 1.64 and 0.92, respectively. The elemental ratio of various GGBS pastes suggests multiple gels such as CASH, NASH, CSH, and (C, N)-ASH are responsible for high mortar compressive strength. In the MK paste, Ca/(Si + Al) and Na/(Si + Al) ratio were 0.0 and 0.21, respectively. Also, the ratios such as Ca/Si, Na/Al, Na/Si and Ca/Al were 0.00, 0.47, 0.40 and 0.00, respectively. The gel produced on activation of MK showed no presence of CASH or CSH in the system. The binder system primarily contained NASH gel, reflecting the lower compressive strength than other pastes studied [67]. The Si/Al ratio of the alkali-activated FA and MK were 3.07 and 1.17, respectively. The higher the Si/Al ratio, the higher the compressive strength, which is observed in the case of GGBS and OPC pastes with Si/Al ratios of 3.06 and 4.06, respectively.

EDX mapping was carried out to map elements in the paste system and is shown in Figure 12. In the alkali-activated fly-ash paste, Na, Si, Al, and Ca were mapped. Si and Al color intensities are higher than Na and Ca, while the Ca has the least intensity. For the GGBS paste, the intensity of all the elements, such as Na, Si, Al, and Ca, is equally

distributed throughout the spectrum area. In the MK paste, the mapped elements show the high intensity of Si and Al but the lower intensity of Ca elements. Lastly, Ca, Si, and Al elements are seen in the OPC paste with a higher Ca intensity. The ternary plot of Ca vs. Al vs. Si and Na vs. Al vs. Si is illustrated in Figures 13 and 14.

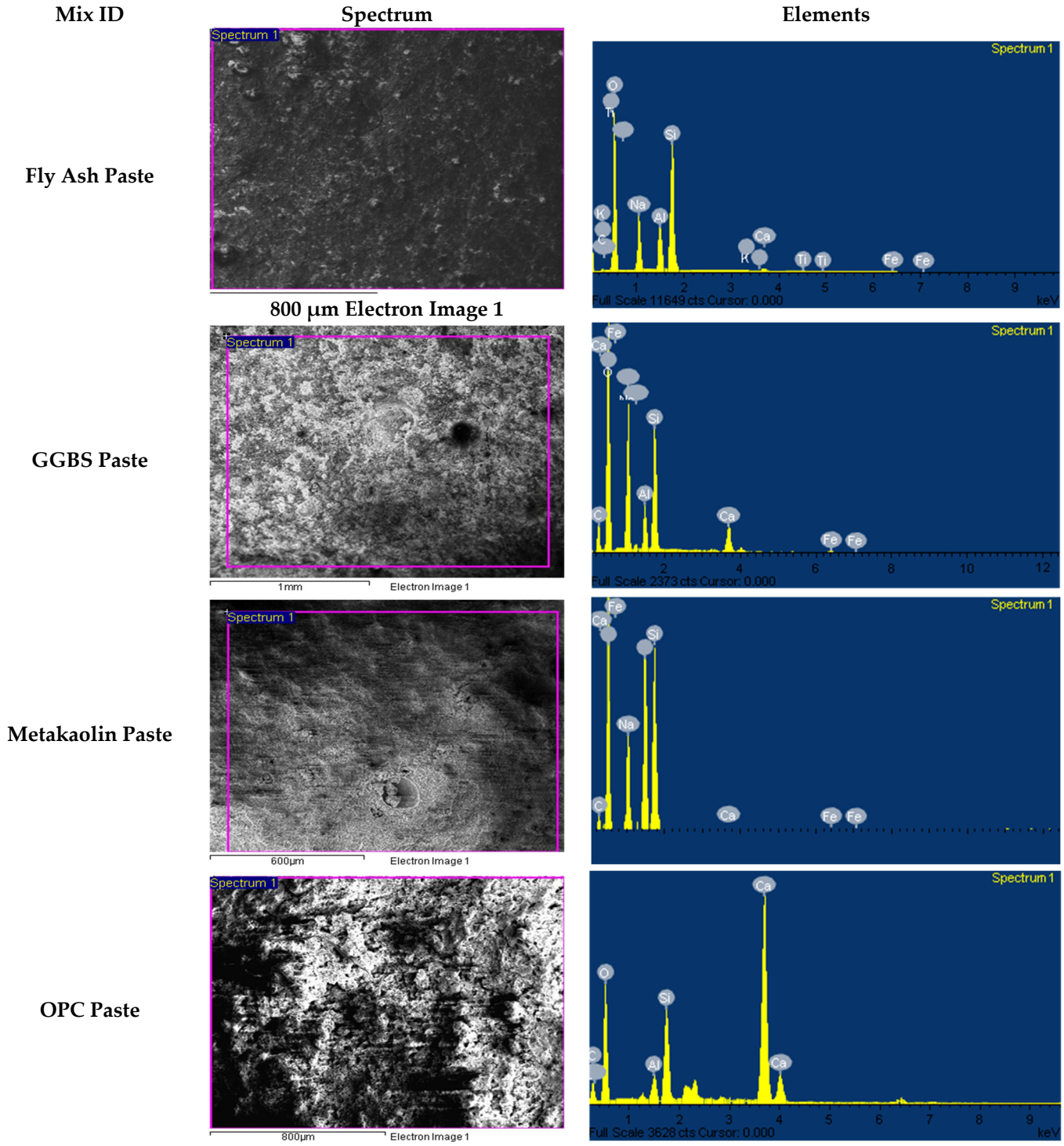

Figure 11. EDX spectrum of pastes at 7 days.

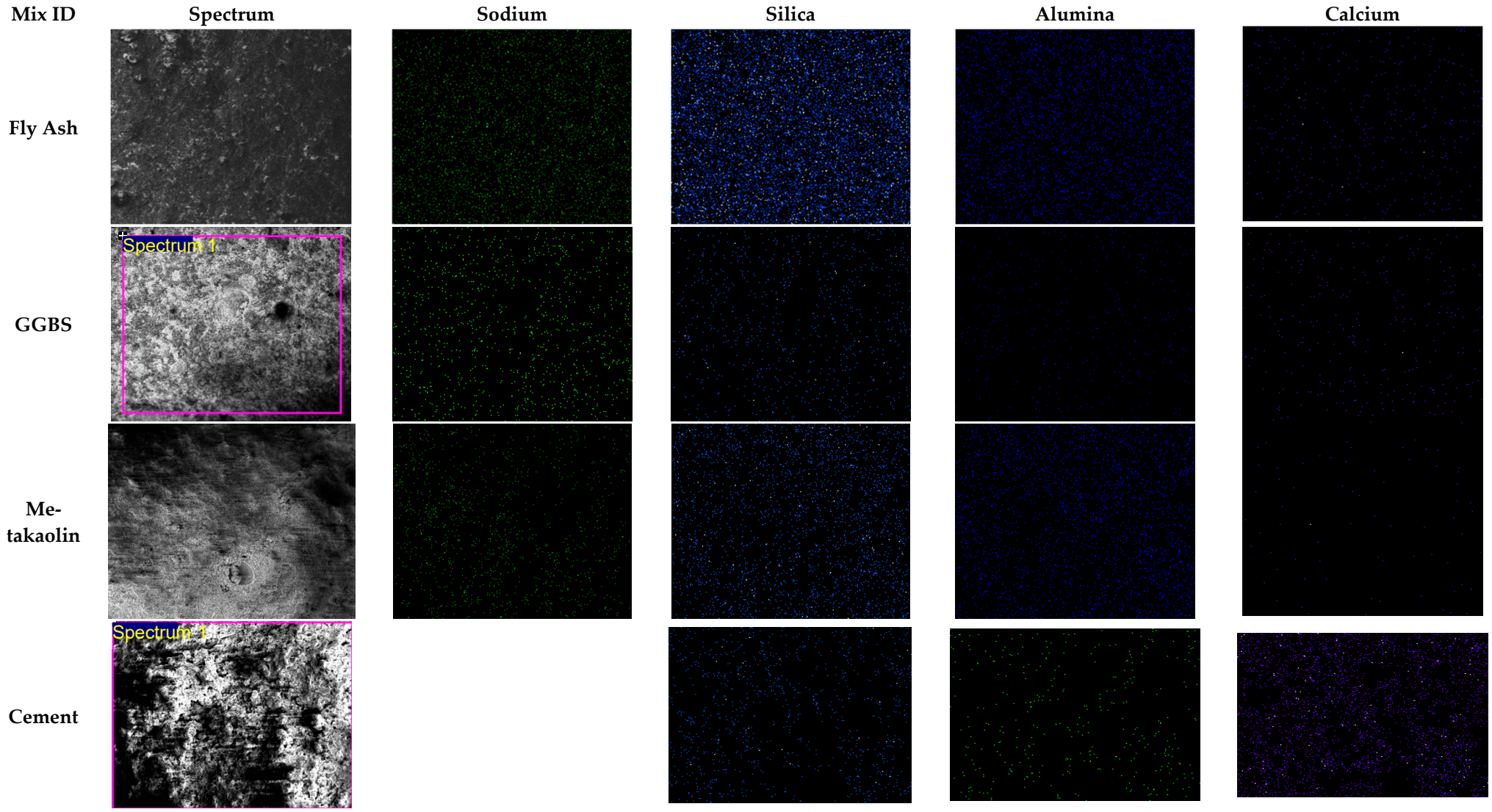

Figure 12. EDS mapping of elements of pastes.

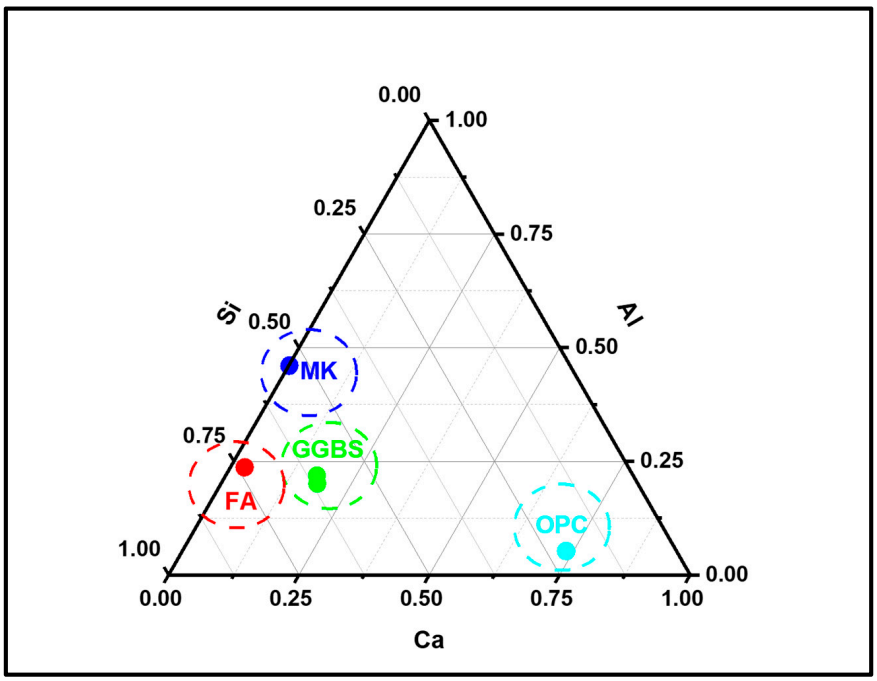

Figure 13. Ternary plot of Ca vs. Al vs. Si.

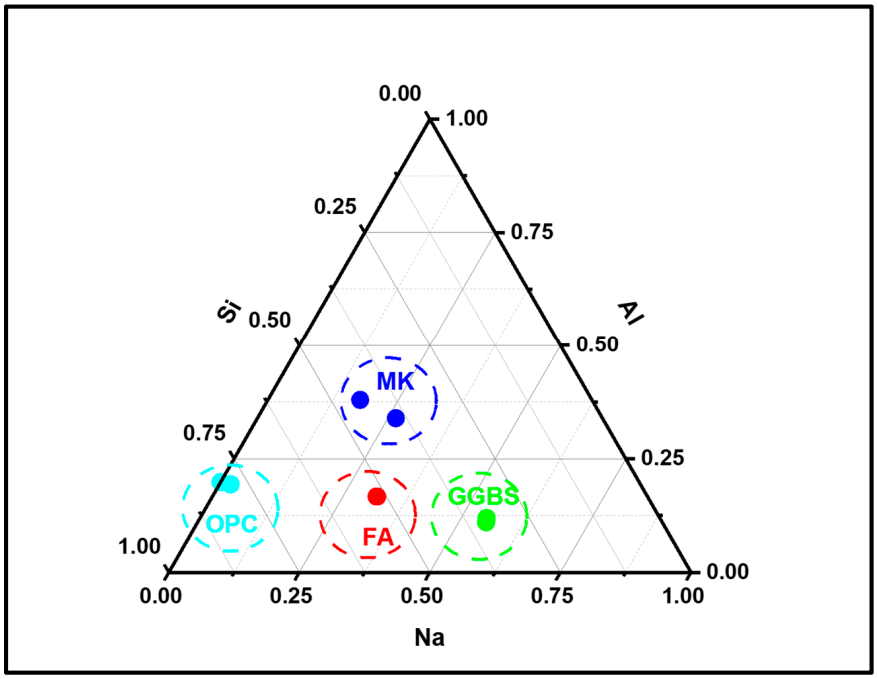

Figure 14. Ternary plot of Na vs. Al vs. Si.

3.3.3. Alkali-Activated FA, GGBS, and MK Studied Using XRD

The chemical composition of the paste specimens after a seven-day ambient curing were identified by XRD. Figures 15–17 show the XRD results for materials such as alkali-activated FA, GGBS, and MK, respectively, and Figure 18 shows the results for the OPC paste. The base binders were transformed into complex crystalline peaks on the FA, GGBS, and MK activation. FA and MK have more impurities in the compounds present in the system than the GGBS and OPC paste.

The quartz chemical compound is mainly an inert crystalline mineral in alkali-activated FA and MK. The peak of SiO_2 is observed at 26.70°, and 26.56° in the FA and MK

pastes. The compounds present in the alkali-activated FA are quartz Si_3O_6, Reyrite $Na_{1.6}Ca_{14}Si_{22}Al_2O_{72}H_8$, and natrolite $Na_{16}Al_{16}Si_{24}O_{96}H_{32}$; the PDF number is shown in Table 6. With the higher content of silica-alumina and low calcium in the FA, after the activation with the water glass solution (NaOH-Na_2SiO_3), the system was transformed into the 3D NASH structure. MK pastes' activation resulted in the development of compounds such as NASH $Na_{32}Si_{64}H_{32}O_{160}$ and $Na_{24}Si_8H_{40}O_{48}$, quartz Si_3O_6, and sillimanite $Al_8Si_4O_{20}$. The NASH peaks were observed at 27.06°,32.47° and sillimanite peaks were positioned at 31.22°, 33.54° in the MK pastes.

In the alkali-activated high calcium (GGBS paste), the compounds present were chabazite $Ca_6Al_{12}Si_{24}O_{108}H_0$ and clinotobermorite $Ca_5Si_6O_{18}H_0$. The chabazite and cinotobermorite peaks are observed at 29.85° and 30.90°, respectively. Finally, the OPC paste hydration products are clinotobermorite, Portlandite, ettringite, vaterite, calcite, and quartz, which were observed at 29.34°, 34.02°,32.64°, 27.62°,28.58° and 26.95° respectively. The molecular structure of CSH, CASH, NASH, and N, C-ASH, is shown in Figure 19 as obtained from High Score Software Plus. The CSH and CASH are cubic molecular structures, while NASH and N, C-ASH are rhombohedral molecular structures [68–70].

Table 6. Compound Name and Chemical Formula used in the XRD.

Samples	PDF Card No.	Compound Name	Chem. Formula
Fly Ash			
	96-900-9667	Quartz	Si_3O_6
	96-900-9471	Reyerite	$Na_{1.6}Ca_{14}Si_{22}Al_2O_{72}H_8$
	96-900-5048	Natrolite	$Na_{16}Al_{16}Si_{24}O_{96}H_{32}$
GGBS			
	96-101-1270	Chabazite	$Ca_6Al_{12}Si_{24}O_{108}H_0$
	96-100-0047	Clinotobermorite	$Ca_5Si_6O_{18}H_0$
MK			
	96-153-3379	NASH	$Na_{32}Si_{64}H_{32}O_{160}$
	96-210-7160	NASH	$Na_{24}Si_8H_{40}O_{48}$
	96-901-2602	Quartz	Si_3O_6
	96-900-1409	Sillimanite	$Al_8Si_4O_{20}$
OPC	96-100-0047	Clinotobermorite	$Ca_5Si_6O_{18}H_0$
	96-100-8782	Portlandite	$Ca_1O_2H_2$
	96-901-5085	Ettringite	$Ca_{12}Al_4S_6O_{100}$ H_{128}
	96-901-6216	Vaterite	Ca4.00 C4.00 O12.00

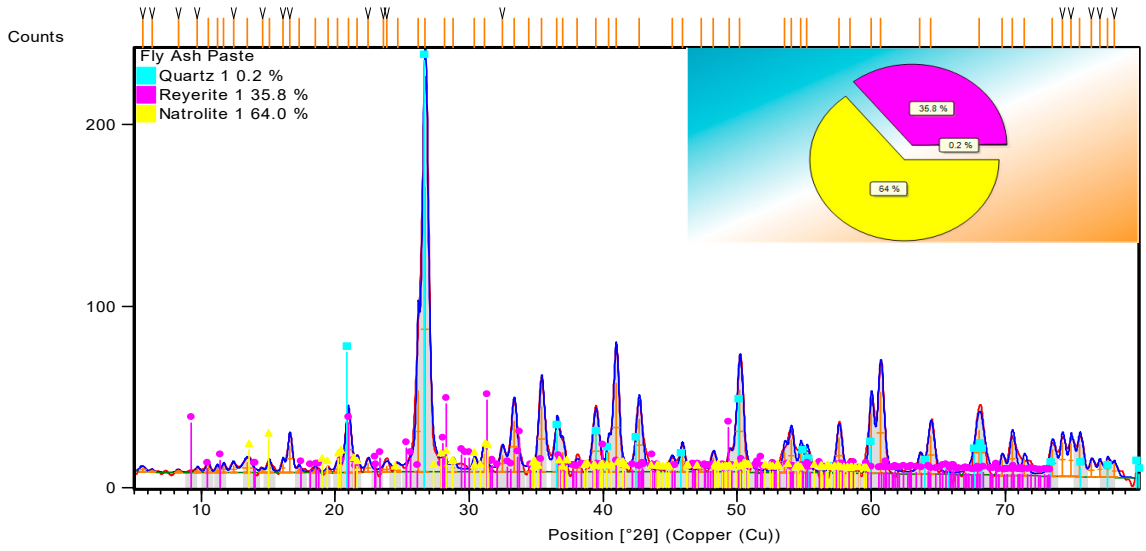

Figure 15. XRD of Fly ash paste at 7 days of ambient curing.

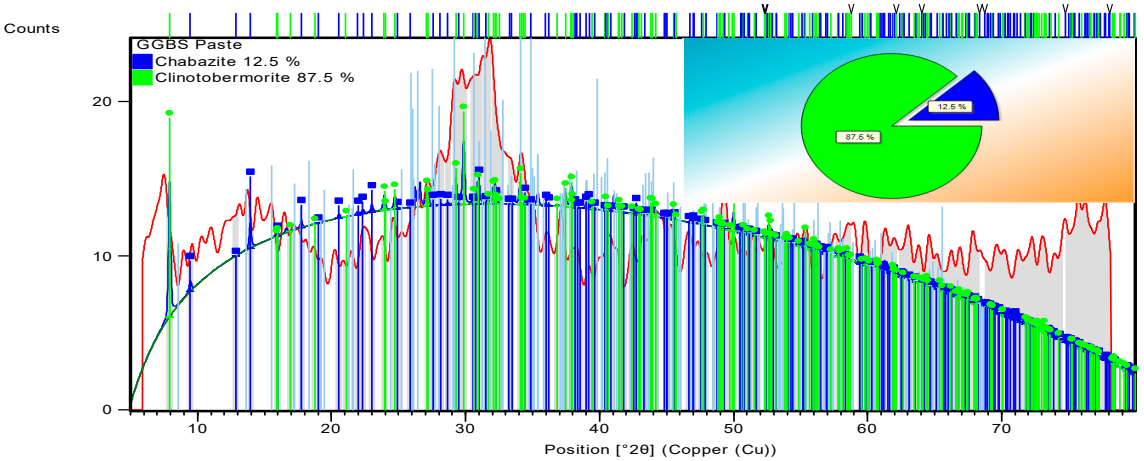

Figure 16. XRD of GGBS paste at 7th days of ambient-curing.

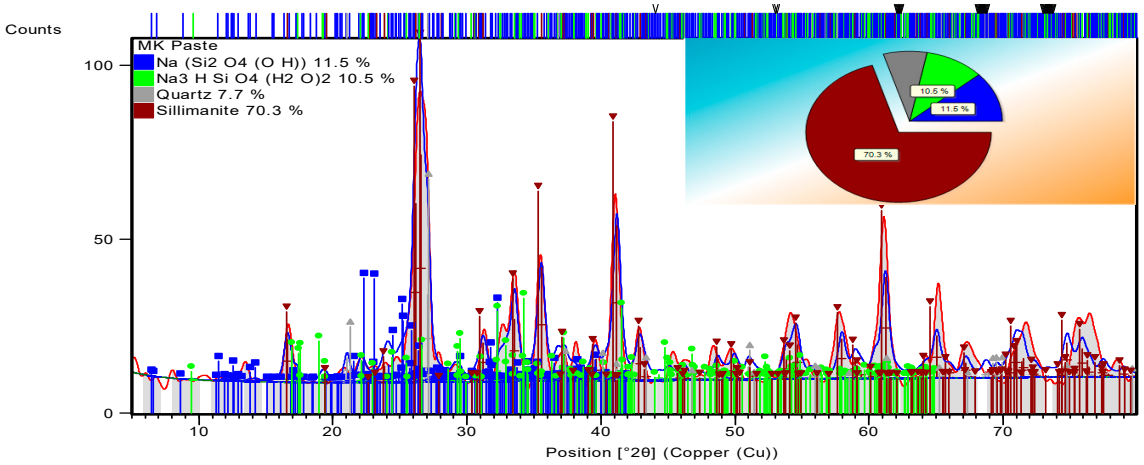

Figure 17. XRD of Metakaolin paste at 7 days of ambient curing.

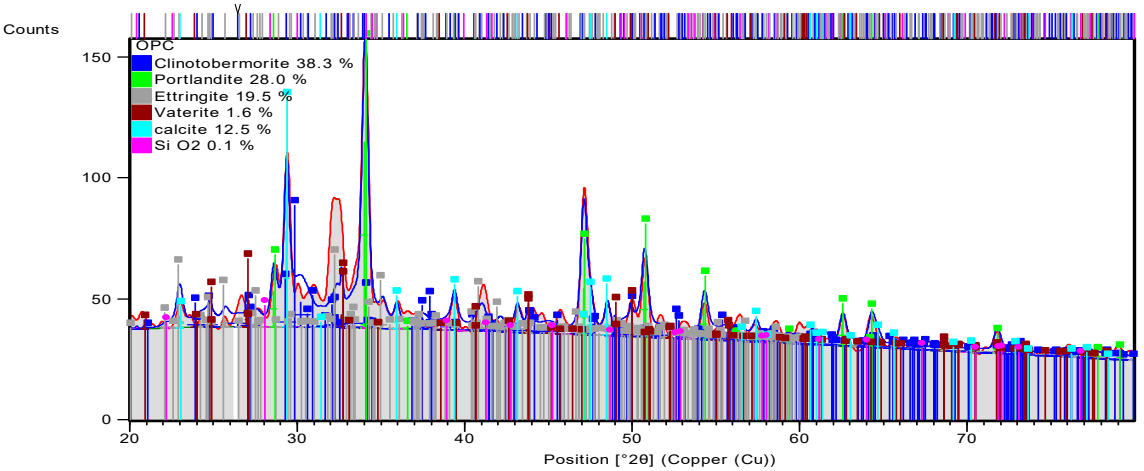

Figure 18. XRD of OPC paste at 7 days of ambient curing.

3.3.4. Alkali-Activated FA, GGBS and MK Studied Using FTIR

Fourier transform infrared spectroscopy (FTIR) was performed to find the chemical bond present in the low-calcium and high-calcium paste cured at seven days. FTIR spectra of the low calcium (FA and MK) and high calcium (GGBS and OPC) paste are shown in Figure 20. The presence of various chemical bonds in the pastes included H-OH (bending and stretching band), OCO (absorption band), TOT (T: tetrahedral Si or Al), and Si-O-Si

bonds. In FA, GGBS, MK, and OPC, the H-OH water bond is observed at the intensities of 3615, 3634, 3610, and 3336 cm^{-1}, respectively. The structural water bond is noticed at 1664, 1671, and 1659 cm^{-1} for FA, GGBS, and OPC, respectively, while there is no structural water bond in the MK [71].

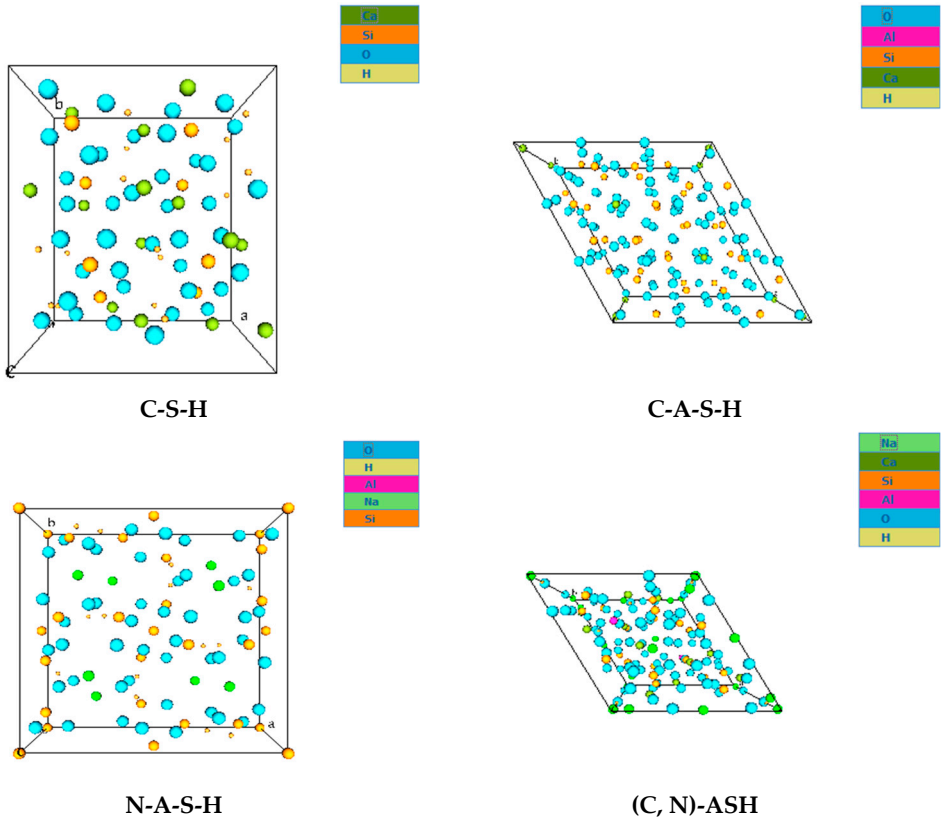

Figure 19. Molecular structure of C-S-H, C-A-S-H, N-A-S-H, and C, N-ASH.

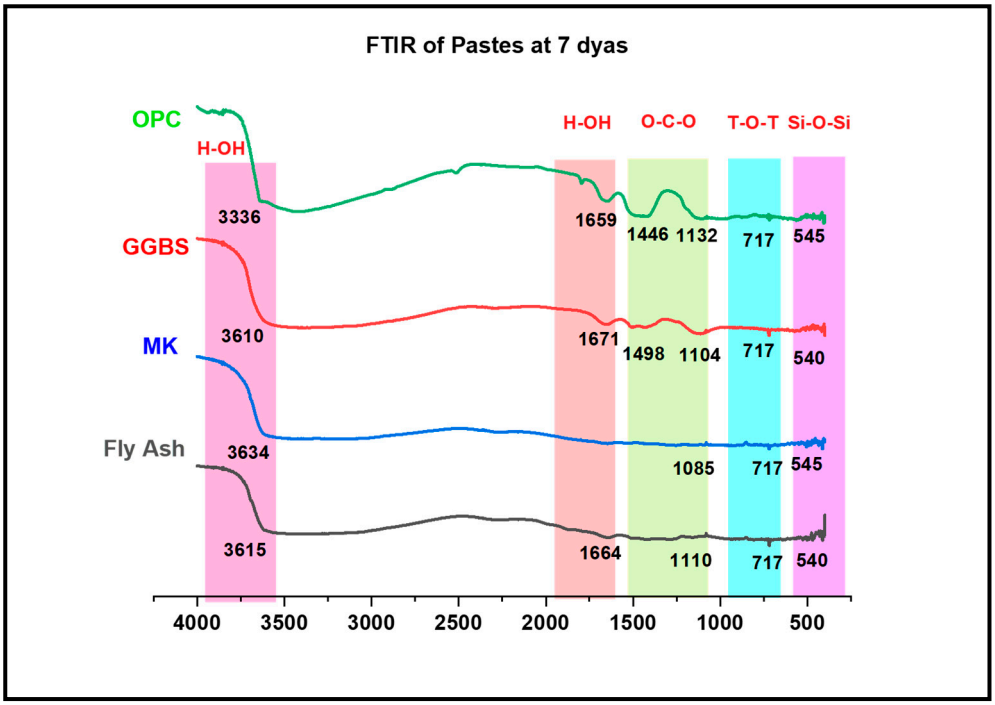

Figure 20. FTIR of Pastes at 7 days of curing.

Sun et al. 2021 studied the variation of white mud in the blend of FA and GGBS. All the aluminosilicate paste samples showed a broad intensity band at roughly 970 cm^{-1}. The vibrations of Si-O-T bands (T: tetrahedral Si or Al) from gel products are responsible for this (1020 cm^{-1} NASH and 950 cm^{-1} CASH). The Al/Si ratio of gel products in AAM is commonly acknowledged as having a significant impact on the wavenumber of the Si-O-T band. The bands are located between 971 and 959 cm^{-1}, which is greater than the wavenumber of the C-A-S-H gel (950 cm^{-1}) and lower than the wavenumber of the NASH gel (i.e., 1020 cm^{-1}), showing the existence of numerous types of gel products [64].

The OCO band was observed in the OPC and GGBS at 1446 and 1498 cm^{-1}, respectively. The existence of the OCO bond is related to carbonate groups, indicating the calcium carbonate compound. Additionally, asymmetric stretching of OCO is related to CO_3^{2-} a bond that shows the carbonation takes place during the ambient curing condition. Si-O-Si or Si-O-Al or Al-O-Al bonds are present in the OPC, GGBS, MK, and FA at the intensity of 1132, 1104, 1085, and 1110 cm^{-1}. Si-O bond also suggests the presence of the silicate glass group, which developed due to the replacement of $(SiO_4)^{4-}$ to $(AlO_4)^{4-}$. The alkali-activated MK showed the lowest wavenumber at 1085 cm^{-1}, attributed to minimum geo-polymerization; this leads to less compressive strength [21,72,73]. The FTIR results are in strong agreement with the XRD and FESEM interpretations.

4. Conclusions

Studies on the properties of popular aluminosilicate pastes, such as fly ash, GGBS, and MK, activated using a water glass solution cured under ambient conditions, revealed the mechanisms that control the setting and hardening characteristics as well as the strength development mechanisms. The following are the concluding points from the experimental program:

- Alkali-activated FA and MK pastes have a prolonged setting time, whereas the alkali-activated GGBS paste possesses quick-setting characteristics;
- Mortars made of alkali-activated FA and MK binder systems showed lower compressive strength, while slag and OPC-based mortars showed higher compressive strengths. The compressive strength showed that a binder system containing more calcium exhibits superior compressive strength;
- UPV values of mortar prepared with alkali-activated FA and MK based binders showed lower values, which means the matrix is less dense. The alkali-activated GGBS mortar-prepared binder had values of UPV slightly higher than that of the OPC-based mortar;
- FESEM images indicated the presence of NASH gel in the low calcium pastes such as FA and MK, and the CASH gel dominated in the slag-based high-calcium system. The CASH gel was characterized by a compact morphology, while the NASH gel displayed a fragmented morphology and contains unreacted particles;
- EDX elemental analysis revealed the Ca/(Si + Al), Na/(Si + Al), Ca/Si, Na/Al, Na/Si, and Ca/Al ratios that define the binder paste's efficacy in comparison to OPC. The presence of NASH gel was observed in fly ash and MK, whereas multiple gel types in the GGBS such as CASH, NASH, C, NASH, and CSH were noted. EDX mapping of the paste also showed a similar pattern;
- XRD and FTIR confirmed the existence of NASH in the FA and MK and (C, N)-ASH in the GGBS paste was present only in traces.

Future Scope

Future studies can be extended to understand the rheological properties of the aluminosilicate paste. Thermodynamic modelling, hydration modelling, and nanoindentation can be carried out to understand the paste's thermodynamics and properties. The durability of other natural pozzolanic pastes is another aspect that can provide more insight and improve applicability.

Author Contributions: Conceptualization, M.K. and S.P.; Methodology, M.K. and S.P.; Software, M.K.; Validation, M.K. and R.R.; Formal analysis, M.K.; Investigation, M.K.; Resources, M.K.; Data curation, M.K.; Writing—original draft, M.K.; Writing—review & editing, M.K., S.P. and R.R.; Visualization, M.K.; Supervision, S.P.; Project administration, M.K. All authors have read and agreed to the published version of the manuscript.

Funding: This research received no external funding.

Data Availability Statement: The data presented in this study are available on request from the corresponding author.

Acknowledgments: First: the authors are thankful to the Department of Civil Engineering, Manipal Institute of Technology, MAHE, Manipal, Karnataka, India. The authors also thank Murari M S, Scientific Officer, DST-PURSE Program Mangalore University, for performing FE-SEM and EDS equipment. The authors would also like to acknowledge for XRD and FT-IR to central institute facility, Manipal Institute of Technology, MAHE and DST-FIST program, Department of Atomic and Molecular Physics, Manipal Institute of Technology, MAHE.

Conflicts of Interest: The authors declare no conflict of interest.

References

1. Okoye, F.N.; Prakash, S.; Singh, N.B. Durability of Fly Ash Based Geopolymer Concrete in the Presence of Silica Fume. *J. Clean. Prod.* **2017**, *149*, 1062–1067. [CrossRef]
2. Zannerni, G.M.; Fattah, K.P.; Al-Tamimi, A.K. Ambient-Cured Geopolymer Concrete with Single Alkali Activator. *Sustain. Mater. Technol.* **2020**, *23*, e00131. [CrossRef]
3. Mendes, B.C.; Pedroti, L.G.; Vieira, C.M.F.; Marvila, M.; Azevedo, A.R.G.; Franco de Carvalho, J.M.; Ribeiro, J.C.L. Application of Eco-Friendly Alternative Activators in Alkali-Activated Materials: A Review. *J. Build. Eng.* **2021**, *35*, 102010. [CrossRef]
4. König, K.; Traven, K.; Pavlin, M.; Ducman, V. Evaluation of Locally Available Amorphous Waste Materials as a Source for Alternative Alkali Activators. *Ceram. Int.* **2021**, *47*, 4864–4873. [CrossRef]
5. Gavali, H.R.; Bras, A.; Faria, P.; Ralegaonkar, R.V. Development of Sustainable Alkali-Activated Bricks Using Industrial Wastes. *Constr. Build. Mater.* **2019**, *215*, 180–191. [CrossRef]
6. Dong, M.; Elchalakani, M.; Karrech, A. Development of High Strength One-Part Geopolymer Mortar Using Sodium Metasilicate. *Constr. Build. Mater.* **2020**, *236*, 117611. [CrossRef]
7. Vo, D.H.; Hwang, C.L.; Yehualaw, M.D.; Liao, M.C. The Influence of MgO Addition on the Performance of Alkali-Activated Materials with Slag−rice Husk Ash Blending. *J. Build. Eng.* **2021**, *33*, 101605. [CrossRef]
8. Habert, G. *Assessing the Environmental Impact of Conventional and "Green" Cement Production*; Woodhead Publishing: Sawston, UK, 2013; ISBN 9780857097675.
9. Zhang, J.; Tan, H.; Bao, M.; Liu, X.; Luo, Z.; Wang, P. Low Carbon Cementitious Materials: Sodium Sulfate Activated Ultra-Fine Slag/Fly Ash Blends at Ambient Temperature. *J. Clean. Prod.* **2021**, *280*, 124363. [CrossRef]
10. Adesanya, E.; Perumal, P.; Luukkonen, T.; Yliniemi, J.; Ohenoja, K.; Kinnunen, P.; Illikainen, M. Opportunities to Improve Sustainability of Alkali-Activated Materials: A Review of Side-Stream Based Activators. *J. Clean. Prod.* **2021**, *286*, 125558. [CrossRef]
11. Shetty, P.P.; Rao, A.U.; Pai, B.H.V.; Kamath, M. V Performance of High-Strength Concrete with the Effects of Seashell Powder as Binder Replacement and Waste Glass Powder as Fine Aggregate. *J. Compos. Sci.* **2023**, *7*, 92. [CrossRef]
12. Madurwar, M.V.; Ralegaonkar, R.V.; Mandavgane, S.A. Application of Agro-Waste for Sustainable Construction Materials: A Review. *Constr. Build. Mater.* **2013**, *38*, 872–878. [CrossRef]
13. Tantri, A.; Nayak, G.; Kamath, M.; Shenoy, A.; Shetty, K.K. Utilization of Cashew Nut-Shell Ash as a Cementitious Material for the Development of Reclaimed Asphalt Pavement Incorporated Self Compacting Concrete. *Constr. Build. Mater.* **2021**, *301*, 124197. [CrossRef]
14. Davidovits, J. *Geopolymer Chemistry and Applications*, 5th, ed.; Geopolymer Publishing: Hauppauge, NY, USA, 2020.
15. Li, C.; Sun, H.; Li, L. A Review: The Comparison between Alkali-Activated Slag (Si + Ca) and Metakaolin (Si + Al) Cements. *Cem. Concr. Res.* **2010**, *40*, 1341–1349. [CrossRef]
16. Flatt, R.J.; Roussel, N.; Cheeseman, C.R. Concrete: An Eco Material That Needs to Be Improved. *J. Eur. Ceram. Soc.* **2012**, *32*, 2787–2798. [CrossRef]
17. Alnahhal, M.F.; Kim, T.; Hajimohammadi, A. Waste-Derived Activators for Alkali-Activated Materials: A Review. *Cem. Concr. Compos.* **2021**, *118*, 103980. [CrossRef]
18. Zhang, Z.H.; Zhu, H.J.; Zhou, C.H.; Wang, H. Geopolymer from Kaolin in China: An Overview. *Appl. Clay Sci.* **2016**, *119*, 31–41. [CrossRef]
19. Bhagath Singh, G.V.P.; Subramaniam, K.V.L. Quantitative XRD Study of Amorphous Phase in Alkali Activated Low Calcium Siliceous Fly Ash. *Constr. Build. Mater.* **2016**, *124*, 139–147. [CrossRef]

20. Jagadisha, A.; Rao, K.B.; Nayak, G.; Kamath, M. Influence of Nano-Silica on the Microstructural and Mechanical Properties of High-Performance Concrete of Containing EAF Aggregate and Processed Quarry Dust. *Constr. Build. Mater.* **2021**, *304*, 124392. [CrossRef]
21. Alventosa, K.M.L.; White, C.E. The Effects of Calcium Hydroxide and Activator Chemistry on Alkali-Activated Metakaolin Pastes. *Cem. Concr. Res.* **2021**, *145*, 106453. [CrossRef]
22. Davidovits, J. Geopolymers: Ceramic-like Inorganic Polymers. *J. Ceram. Sci. Technol.* **2017**, *8*, 335–350. [CrossRef]
23. Ruiz-Santaquiteria, C.; Fernández-Jiménez, A.; Palomo, A. Alternative Prime Materials for Developing New Cements: Alkaline Activation of Alkali Aluminosilicate Glasses. *Ceram. Int.* **2016**, *42*, 9333–9340. [CrossRef]
24. Gavali, H.R.; Ralegaonkar, R.V. Design Development of Sustainable Alkali-Activated Bricks. *J. Build. Eng.* **2020**, *30*, 101302. [CrossRef]
25. Wang, Y.; Liu, X.; Zhang, W.; Li, Z.; Zhang, Y.; Li, Y.; Ren, Y. Effects of Si/Al Ratio on the Efflorescence and Properties of Fly Ash Based Geopolymer. *J. Clean. Prod.* **2020**, *244*, 118852. [CrossRef]
26. Khan, K.A.; Raut, A.; Chandrudu, C.R.; Sashidhar, C. Design and Development of Sustainable Geopolymer Using Industrial Copper Byproduct. *J. Clean. Prod.* **2021**, *278*, 123565. [CrossRef]
27. Puligilla, S.; Mondal, P. Co-Existence of Aluminosilicate and Calcium Silicate Gel Characterized through Selective Dissolution and FTIR Spectral Subtraction. *Cem. Concr. Res.* **2015**, *70*, 39–49. [CrossRef]
28. Rao, A.U.; Bhandary, R.; Maddodi, B.; Tantri, A.; Shenoy, S.; Kamath, M.; Shetty, R.S. Performance Evaluation of Hybrid Glass Wastes Incorporated Concrete. *Eng. Sci.* **2022**, *20*, 188–198. [CrossRef]
29. Zhang, P.; Wang, K.; Li, Q.; Wang, J.; Ling, Y. Fabrication and Engineering Properties of Concretes Based on Geopolymers/Alkali-Activated Binders—A Review. *J. Clean. Prod.* **2020**, *258*, 120896. [CrossRef]
30. Xu, H.; Van Deventer, J.S.J. The Geopolymerisation of Alumino-Silicate Minerals. *Int. J. Miner. Process.* **2000**, *59*, 247–266. [CrossRef]
31. Zhao, D.; Khoshnazar, R. Microstructure of Cement Paste Incorporating High Volume of Low-Grade Metakaolin. *Cem. Concr. Compos.* **2020**, *106*, 103453. [CrossRef]
32. Wardhono, A.; Gunasekara, C.; Law, D.W.; Setunge, S. Comparison of Long Term Performance between Alkali Activated Slag and Fly Ash Geopolymer Concretes. *Constr. Build. Mater.* **2017**, *143*, 272–279. [CrossRef]
33. Kumar, M.; Shreelaxmi, P.; Kamath, M. *Review on Characteristics of Sewage Sludge Ash and Its Partial Replacement as Binder Material in Concrete*; Springer: Berlin/Heidelberg, Germany, 2021; Volume 105, ISBN 9789811582929.
34. Kamath, M.V.; Prashanth, S.; Kumar, M. Review of Low to High Strength Alkali-Activated and Geopolymer Concrete. In *Lecture Notes in Civil Engineering*; Springer: Singapore, 2021; pp. 105–113, ISBN 9789811582929.
35. Alnahhal, M.F.; Kim, T.; Hajimohammadi, A. Distinctive Rheological and Temporal Viscoelastic Behaviour of Alkali-Activated Fly Ash/Slag Pastes: A Comparative Study with Cement Paste. *Cem. Concr. Res.* **2021**, *144*, 106441. [CrossRef]
36. Li, Z.; Wyrzykowski, M.; Dong, H.; Granja, J.; Azenha, M.; Lura, P.; Ye, G. Internal Curing by Superabsorbent Polymers in Alkali-Activated Slag. *Cem. Concr. Res.* **2020**, *135*, 106123. [CrossRef]
37. Xu, C.; Ni, W.; Li, K.; Zhang, S.; Xu, D. Activation Mechanisms of Three Types of Industrial By-Product Gypsums on Steel Slag–Granulated Blast Furnace Slag-Based Binders. *Constr. Build. Mater.* **2021**, *288*, 123111. [CrossRef]
38. Gao, X.; Yu, Q.L.; Brouwers, H.J.H. Properties of Alkali Activated Slag-Fly Ash Blends with Limestone Addition. *Cem. Concr. Compos.* **2015**, *59*, 119–128. [CrossRef]
39. Gao, X.; Yu, Q.L.; Brouwers, H.J.H. Characterization of Alkali Activated Slag-Fly Ash Blends Containing Nano-Silica. *Constr. Build. Mater.* **2015**, *98*, 397–406. [CrossRef]
40. Li, Z.; Liang, X.; Chen, Y.; Ye, G. Effect of Metakaolin on the Autogenous Shrinkage of Alkali-Activated Slag-Fly Ash Paste. *Constr. Build. Mater.* **2021**, *278*, 122397. [CrossRef]
41. Kamath, M.V.; Prashanth, S.; Kumar, M.; Tantri, A. Machine-Learning-Algorithm to Predict the High-Performance Concrete Compressive Strength Using Multiple Data. *J. Eng. Des. Technol.* **2021**. [CrossRef]
42. Kumar, M.; Prashant, S.; Kamath, M.V. Enhancing the Sustainability of High Strength Concrete in Terms of Embodied Energy and Carbon Emission by Incorporating Sewage Sludge and Fly Ash. *Innov. Infrastruct. Solut.* **2022**, *7*, 240. [CrossRef]
43. Kamath, M.; Prashant, S.; Kumar, M. Micro-Characterisation of Alkali Activated Paste with Fly Ash-GGBS-Metakaolin Binder System with Ambient Setting Characteristics. *Constr. Build. Mater.* **2021**, *277*, 122323. [CrossRef]
44. *ASTM C618-12*; Standard Specification for Coal Fly Ash and Raw or Calcined Natural Pozzolan for Use. ASTM: West Conshohocken, PA, USA, 2010; pp. 3–6. [CrossRef]
45. *IS 383:2016*; IS383 Coarse and Fine Aggregate for Concrete, 3rd ed. BIS: Delhi, India, 2016; pp. 1–17.
46. *ASTM Standards C191-04*; Time of Setting of Hydraulic Cement by Vicat Needle. ASTM: West Conshohocken, PA, USA, 2008; pp. 1–10. [CrossRef]
47. *ASTM C109/C109M-16a*; Standard Test Method for Compressive Strength of Hydraulic Cement Mortars (Using 2-in. or [50-mm] Cube Specimens). ASTM: West Conshohocken, PA, USA, 2016.
48. *ASTM C597*; Standard Test Method for Pulse Velocity Through Concrete. ASTM: West Conshohocken, PA, USA, 2010; pp. 3–6. [CrossRef]
49. Dai, X.; Aydin, S.; Yardimci, M.Y.; Lesage, K.; de Schutter, G. Influence of Water to Binder Ratio on the Rheology and Structural Build-up of Alkali-Activated Slag/Fly Ash Mixtures. *Constr. Build. Mater.* **2020**, *264*, 120253. [CrossRef]

50. Almakhadmeh, M.; Soliman, A.M. Effects of Mixing Water Temperatures on Properties of One-Part Alkali-Activated Slag Paste. *Constr. Build. Mater.* **2021**, *266*, 121030. [CrossRef]
51. Pham, T.M. Enhanced Properties of High-Silica Rice Husk Ash-Based Geopolymer Paste by Incorporating Basalt Fibers. *Constr. Build. Mater.* **2020**, *245*, 118422. [CrossRef]
52. Abhishek, H.S.; Prashant, S.; Kamath, M.V.; Kumar, M. Fresh Mechanical and Durability Properties of Alkali-Activated Fly Ash-Slag Concrete: A Review. *Innov. Infrastruct. Solut.* **2022**, *7*, 116. [CrossRef]
53. Ng, C.; Alengaram, U.J.; Wong, L.S.; Mo, K.H.; Jumaat, M.Z.; Ramesh, S. A Review on Microstructural Study and Compressive Strength of Geopolymer Mortar, Paste and Concrete. *Constr. Build. Mater.* **2018**, *186*, 550–576. [CrossRef]
54. Naghizadeh, A.; Ekolu, S.O. Method for Comprehensive Mix Design of Fly Ash Geopolymer Mortars. *Constr. Build. Mater.* **2019**, *202*, 704–717. [CrossRef]
55. Zhang, H.Y.; Liu, J.C.; Wu, B. Mechanical Properties and Reaction Mechanism of One-Part Geopolymer Mortars. *Constr. Build. Mater.* **2021**, *273*, 121973. [CrossRef]
56. Xu, L.Y.; Alrefaei, Y.; Wang, Y.S.; Dai, J.G. Recent Advances in Molecular Dynamics Simulation of the N-A-S-H Geopolymer System: Modeling, Structural Analysis, and Dynamics. *Constr. Build. Mater.* **2021**, *276*, 122196. [CrossRef]
57. Garcia-Lodeiro, I.; Palomo, A.; Fernández-Jiménez, A.; MacPhee, D.E. Compatibility Studies between N-A-S-H and C-A-S-H Gels. Study in the Ternary Diagram Na_2O-CaO-Al_2O_3-SiO 2-H_2O. *Cem. Concr. Res.* **2011**, *41*, 923–931. [CrossRef]
58. Cercel, J.; Adesina, A.; Das, S. Performance of Eco-Friendly Mortars Made with Alkali-Activated Slag and Glass Powder as a Binder. *Constr. Build. Mater.* **2021**, *270*, 121457. [CrossRef]
59. Farhan, N.A.; Sheikh, M.N.; Hadi, M.N.S. Investigation of Engineering Properties of Normal and High Strength Fly Ash Based Geopolymer and Alkali-Activated Slag Concrete Compared to Ordinary Portland Cement Concrete. *Constr. Build. Mater.* **2019**, *196*, 26–42. [CrossRef]
60. Sitarz, M.; Hager, I.; Choińska, M. Evolution of Mechanical Properties with Time of Fly-ash-based Geopolymer Mortars under the Effect of Granulated Ground Blast Furnace Slag Addition. *Energies* **2020**, *13*, 1135. [CrossRef]
61. Abdalqader, A.F.; Jin, F.; Al-Tabbaa, A. Development of Greener Alkali-Activated Cement: Utilisation of Sodium Carbonate for Activating Slag and Fly Ash Mixtures. *J. Clean. Prod.* **2016**, *113*, 66–75. [CrossRef]
62. Zhang, S.; Li, Z.; Ghiassi, B.; Yin, S.; Ye, G. Fracture Properties and Microstructure Formation of Hardened Alkali-Activated Slag/Fly Ash Pastes. *Cem. Concr. Res.* **2021**, *144*, 106447. [CrossRef]
63. Cao, Y.F.; Tao, Z.; Pan, Z.; Wuhrer, R. Effect of Calcium Aluminate Cement on Geopolymer Concrete Cured at Ambient Temperature. *Constr. Build. Mater.* **2018**, *191*, 242–252. [CrossRef]
64. Zhang, Y.; Wan, X.; Hou, D.; Zhao, T.; Cui, Y. The Effect of Mechanical Load on Transport Property and Pore Structure of Alkali-Activated Slag Concrete. *Constr. Build. Mater.* **2018**, *189*, 397–408. [CrossRef]
65. Li, Z.; Li, S. Effects of Wetting and Drying on Alkalinity and Strength of Fly Ash/Slag-Activated Materials. *Constr. Build. Mater.* **2020**, *254*, 119069. [CrossRef]
66. Lothenbach, B.; Kulik, D.A.; Matschei, T.; Balonis, M.; Baquerizo, L.; Dilnesa, B.; Miron, G.D.; Myers, R.J. Cemdata18: A Chemical Thermodynamic Database for Hydrated Portland Cements and Alkali-Activated Materials. *Cem. Concr. Res.* **2019**, *115*, 472–506. [CrossRef]
67. Marathe, S.; Mithanthaya, I.R.; Shenoy, R.Y. Durability and Microstructure Studies on Slag-Fly Ash-Glass Powder Based Alkali Activated Pavement Quality Concrete Mixes. *Constr. Build. Mater.* **2021**, *287*, 123047. [CrossRef]
68. Sun, R.; Fang, C.; Zhang, H.; Ling, Y.; Feng, J.; Qi, H.; Ge, Z. Chemo-Mechanical Properties of Alkali-Activated Slag/Fly Ash Paste Incorporating White Mud. *Constr. Build. Mater.* **2021**, *291*, 123312. [CrossRef]
69. Salih, M.A.; Abang Ali, A.A.; Farzadnia, N. Characterization of Mechanical and Microstructural Properties of Palm Oil Fuel Ash Geopolymer Cement Paste. *Constr. Build. Mater.* **2014**, *65*, 592–603. [CrossRef]
70. Jagadisha; Balakrishna Rao, K.; Nayak, G.; Adithya Shenoy, B. *A Review on Properties of Sustainable Concrete Using Iron and Steel Slag Aggregate as Replacement for Natural Aggregate*; Springer: Singapore, 2021; Volume 105, ISBN 9789811582929.
71. Wang, R.; Wang, J.; Dong, T.; Ouyang, G. Structural and Mechanical Properties of Geopolymers Made of Aluminosilicate Powder with Different SiO2/Al2O3 Ratio: Molecular Dynamics Simulation and Microstructural Experimental Study. *Constr. Build. Mater.* **2020**, *240*, 117935. [CrossRef]
72. Zerzouri, M.; Bouchenafa, O.; Hamzaoui, R.; Ziyani, L.; Alehyen, S. Physico-Chemical and Mechanical Properties of Fly Ash Based-Geopolymer Pastes Produced from Pre-Geopolymer Powders Obtained by Mechanosynthesis. *Constr. Build. Mater.* **2021**, *288*, 123135. [CrossRef]
73. Lin, H.; Liu, H.; Li, Y.; Kong, X. Properties and Reaction Mechanism of Phosphoric Acid Activated Metakaolin Geopolymer at Varied Curing Temperatures. *Cem. Concr. Res.* **2021**, *144*, 106425. [CrossRef]